DESIGN AND SIMULATION OF CIRCULAR ARRAYS OF TRAPEZOIDAL-TOOTH LOG-PERIODIC ANTENNAS VIA GENETIC OPTIMIZATION

L. Gürel and Ö. Ergül [†]

Department of Electrical and Electronics Engineering
Bilkent University
TR-06800, Bilkent, Ankara, Turkey

Abstract—Circular arrays of log-periodic (LP) antennas are designed and their operational properties are investigated in a sophisticated simulation environment that is based on the recent advances in computational electromagnetics. Due to the complicated structures of the trapezoidal-tooth array elements and the overall array configuration, their analytical treatments are prohibitively difficult. Therefore, the simulation results presented in this paper are essential for their analysis and design. We present the design of a three-element LP array showing broadband characteristics. The directive gain is stabilized in the operation band using optimization by genetic algorithms. We demonstrate that the optimization procedure can also be used to provide beam-steering ability to LP arrays.

1. INTRODUCTION

Although they have been known for about five decades [1–5], log-periodic (LP) antennas are still interesting [6, 7] due to their ability to display quasi-frequency-independent characteristics over a wide band of frequencies. The broadband capability of these antennas has attracted the interest of many researchers. LP dipole arrays [4, 5] have become particularly popular because of their simplified geometries. Numerous reports have appeared in the literature, investigating LP dipole arrays, their operational properties, and various design procedures [8–23]. However, there are relatively few reports on the analysis of other LP structures with more complicated geometries [24–30]. Earlier, we applied the recent advances in computational

[†] The authors are also with Computational Electromagnetics Research Center (BiLCEM), Bilkent University, TR-06800, Bilkent, Ankara, Turkey

electromagnetics to model general LP structures and perform tests on their configurations [31–33]. The results obtained in the simulation environment have led to essential improvements in fundamental design procedures that could not be achieved with textbook-type theoretical approaches alone.
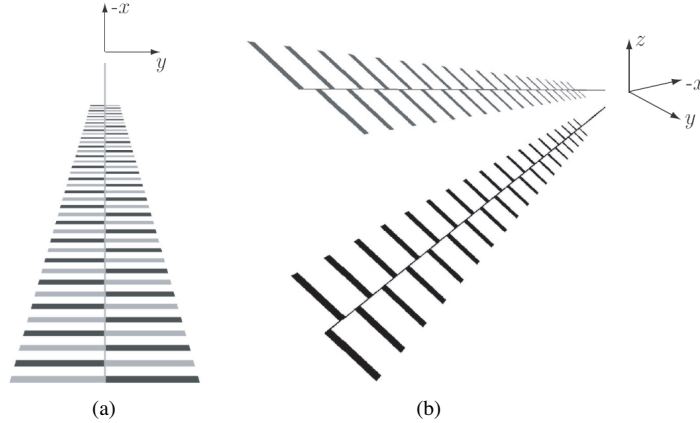

(a)   (b)

Figure 1. Trapezoidal-tooth LP antenna detailed in [32]. (a) Top view, (b) three-dimensional view. This antenna is employed to construct the circular arrays.

In the present study, we use the simulation environment to investigate broadband circular arrays of LP antennas. Figure 1 displays the LP antenna employed as the element of circular arrays. This is a trapezoidal-tooth LP antenna as detailed in [32]; it can operate almost frequency independent from 300 MHz to 800 MHz. The antenna has two arms; each is 1 m long and there is a 45° angle between them. The two arms are physically separated, but they are connected by an excitation source defined in the simulation environment [33]. The length of the elements located on the arms varies from 4 cm to 27 cm. There are 38 elements on each arm, and the expansion angle is 30°, i.e., the elements on an arm grow with an angle of 30°. The geometric growth factor (τ) of the antenna is 0.95 which means that

$$\tau = \frac{R_{i+1}}{R_i} = 0.95, \qquad i = 1, \ldots, 37, \tag{1}$$

where R_i represents the length of the ith element. Therefore, $R_1 = 27$ cm and $R_{38} = 4$ cm.

We employ the LP antenna shown in Figure 1 to construct circular arrays with regularly-spaced elements, as depicted in Figure 2. To preserve frequency independence, the antennas are arranged in a

circular form. In theory, the concept of array factor suggests an optimistic scenario, where frequency independence is conserved in the case of a circular arrangement of the LP antennas. However, our simulations show that mutual couplings between the LP antennas play an important role in shaping the radiation characteristics and that they cannot be ignored. Any analytical treatment that would handle these couplings as well as the other electromagnetic effects would be difficult and would require placing restrictions on the geometry [9]. Therefore, using the simulation environment becomes essential for the analysis of LP arrays.
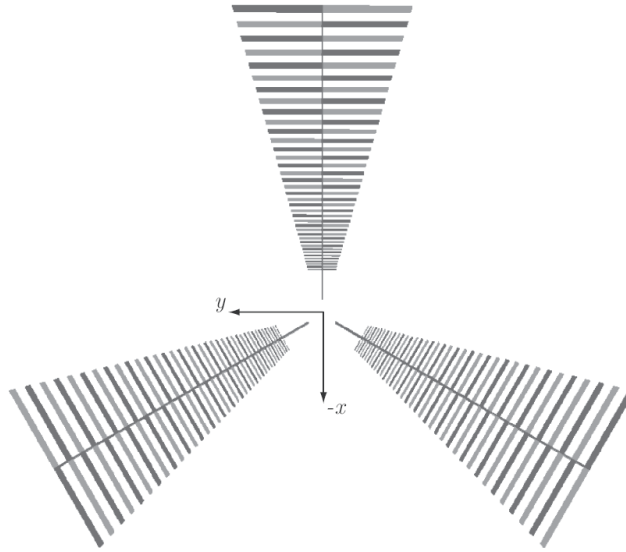

Figure 2. Circular array of LP antennas constructed by employing three identical trapezoidal-tooth antennas depicted in Figure 1. The antennas are regularly spaced.

To add beam-steering ability to the LP arrays, we optimize the radiation pattern and find the relative excitation coefficients to maximize the directive gain. The directive gain in the direction (θ, ϕ) is defined as

$$D(\theta, \phi) = 4\pi \frac{f(\theta, \phi)}{P}, \tag{2}$$

where

$$P = \int_0^{2\pi} \int_0^{\pi} f(\theta, \phi) \sin \theta d\theta d\phi \tag{3}$$

and $f(\theta, \phi)$ represents the radiation intensity. To maximize the directive gain in a given direction, we rotate the main beam in that direction. With optimization, the main beam of the radiation can be steered in some sector centered at a specific angle. Since circular arrays, such as one in Figure 2, are constructed with regularly-spaced elements and are symmetric, the results of an optimization in a sector can also be used in other sectors. Due to the large optimization space, we employed genetic algorithms to perform the optimization. The results of the arrays with three antennas will be presented in this paper although we applied the same procedure also to more populous arrays.

The rest of the paper is organized as follows. In the next section, we outline the theoretical and numerical methods used for electromagnetic modeling. Multiple LP antennas in circular arrangement are introduced in Section 3, and frequency independence is discussed. Then, in Section 4, we explain how the genetic algorithms are used for the optimization of circular arrays. Finally, the results for beam steering are demonstrated in Section 5, and we present conclusions in Section 6.

2. ELECTROMAGNETIC MODELING

In this paper, we model LP antennas and their arrays by using perfectly conducting sheets. The electromagnetic radiation problem in the frequency domain is formulated by employing the electric-field integral equation (EFIE) [34]. This equation is derived from the boundary condition for the tangential electric field, and it can be written in the $\exp(-iwt)$ convention as

$$\hat{\boldsymbol{t}} \cdot \int_{S'} d\boldsymbol{r}' \overline{\boldsymbol{G}}(\boldsymbol{r}, \boldsymbol{r}') \cdot \boldsymbol{J}(\boldsymbol{r}') = \frac{i}{k\eta}\hat{\boldsymbol{t}} \cdot \boldsymbol{E}^{inc}(\boldsymbol{r}), \qquad (4)$$

where the scattered electric field is expressed in terms of the induced current $\boldsymbol{J}$ on the surface of the antenna S'. In (4), $\hat{\boldsymbol{t}}$ is any tangential vector at the observation point $\boldsymbol{r}$, $\boldsymbol{E}^{inc}$ is the incident electric field created by the excitations of the antennas, k is the wavenumber, η is the characteristic impedance of the free space, and

$$\overline{\boldsymbol{G}}(\boldsymbol{r}, \boldsymbol{r}') = \left[\overline{\boldsymbol{I}} + \frac{\nabla\nabla}{k^2}\right] g(\boldsymbol{r}, \boldsymbol{r}') \qquad (5)$$

is the dyadic Green's function based on the scalar Green's function

$$g(\boldsymbol{r}, \boldsymbol{r}') = \frac{e^{ik|\boldsymbol{r}-\boldsymbol{r}'|}}{4\pi|\boldsymbol{r} - \boldsymbol{r}'|} \qquad (6)$$

for the three-dimensional Helmholtz equation.

For the numerical solution of the EFIE in (4) using the method of moments (MOM) [35], the unknown surface current is expanded in a series of basis functions $\boldsymbol{b}_n$ as

$$\boldsymbol{J}(\boldsymbol{r}) = \sum_{n=1}^{N} a_n \boldsymbol{b}_n(\boldsymbol{r}), \tag{7}$$

where a_n is the unknown coefficient of the nth basis function and N is the number of unknowns. The boundary condition in (4) is then projected onto the testing functions $\boldsymbol{t}_m$ to obtain the $N \times N$ matrix equation

$$\sum_{n=1}^{N} Z_{mn}^E a_n = v_m^E, \qquad m = 1, \dots, N, \tag{8}$$

where

$$Z_{mn}^E = \int_{S_m} d\boldsymbol{r}\, \boldsymbol{t}_m(\boldsymbol{r}) \cdot \int_{S_n} d\boldsymbol{r}'\, \overline{\boldsymbol{G}}(\boldsymbol{r}, \boldsymbol{r}') \cdot \boldsymbol{b}_n(\boldsymbol{r}') \tag{9}$$

represents the matrix elements, and

$$v_m^E = \frac{i}{k\eta} \int_{S_m} d\boldsymbol{r}\, \boldsymbol{t}_m(\boldsymbol{r}) \cdot \boldsymbol{E}^{inc}(\boldsymbol{r}) \tag{10}$$

represents the elements of the excitation vector on the right-hand-side of the system in (8). In (9) and (10), S_m and S_n denote the spatial support of the mth testing and nth basis functions, respectively.

For a simultaneous discretization of the integral equation and the geometry of the problem, the surface is meshed by using small (about $\lambda/100$, where λ is the wavelength at the lowest frequency of the operation band of the antenna) planar triangles, on which Rao-Wilton-Glisson (RWG) [36] basis and testing functions are defined. The evaluation of (9) with the RWG functions is widely available in the literature [36]. However, to calculate the excitation vector in (10), we need to find a proper representation for the feed of the antenna. In [32], we achieved this by employing a physical connection, on which a delta-gap source was defined. In the present work, we use a more realistic scenario as detailed in [33], where the current sources are attached to the antenna. This is accomplished by using a pair of half basis functions associated with the feed locations. The resulting excitation vector in (10) is calculated by evaluating the interactions of the two half basis functions with the ordinary (full) basis functions $\boldsymbol{b}_n$ for $n = 1, 2, \dots, N$.

   Although the number of unknowns is relatively low (1000–10,000) and the radiation problems studied in this paper could be solved with MOM, we use an iterative algorithm and employ the multilevel fast multipole algorithm (MLFMA) [37, 38] to speed up the matrix-vector products required during the iterations. Such an acceleration is necessary since multiple solutions are required at several frequencies. Indeed, we use high sampling rate in frequency sweeps so that we can properly observe the rapid oscillations in radiation patterns and directive gains of LP antennas and their array configurations. This leads to about 100 to 1000 solutions per problem, requiring an efficient algorithm, such as MLFMA, to reach solutions quickly without sacrificing accuracy.

3. CIRCULAR ARRAYS OF LP ANTENNAS

Theoretically, a significant majority of the induced current on an LP antenna is on a region of the teeth that is about quarter-wavelength long [39, 40]. This is called the active region, and it moves along the antenna as the frequency changes. For high frequencies, the active region is on the small elements near the feed location; for lower frequencies, it is located on larger elements. The operational frequency range for an LP antenna is directly determined by where the active region is located on the antenna. When the frequency is adjusted so that the active region is completely located on the antenna, the antenna operates properly. However, frequency independence collapses whenever the active region begins to overflow and cannot be accommodated on the antenna. Since the active region is located on more than one element and its size is unknown a priori, it is difficult to calculate the exact bounds for the range of frequency independence. At this stage, simulations of the antenna to calculate the extent of the active region at different frequencies become useful for correcting the design [32].

   Operation range depends on the size of the elements of the LP antenna, and frequency independence in the range is affected by the density of the elements. When the frequency changes, the variation in the radiation characteristics of the antenna can be small if the active region moves smoothly on the antenna. This can be achieved by selecting τ close to unity, as in the LP antenna shown in Figure 1. In general, there is a trade-off between geometric simplicity and frequency independence. For example, when τ drops, the number of elements required for a given bandwidth becomes small; it then becomes easier to construct the antenna with fewer elements. However, frequency independence deteriorates due to the larger gaps between the

consecutive elements, and the resulting non-smooth movement of the active region along the antenna.

When LP antennas are used to construct an array, it is better to arrange them circularly, as shown in Figure 2. In this figure, the three LP antennas in Figure 1 are regularly placed with a 120° angle between each. Theoretically, the radiation intensity of a circular array of identical elements can be calculated as [41]

$$f_a(\theta, \phi) = f_{AF} \times f_e(\theta, \phi), \tag{11}$$

where f_e and f_a represent the radiation intensities of a single element and the array, respectively. This theoretical scenario is illustrated in Figure 3, where the elements are represented by the dots on the circle. The array factor f_{AF} in (11) can be calculated as

$$f_{AF} = \sum_{p=1}^{P} I_p \exp(-ika \sin\theta \cos(\phi - \phi_p)), \tag{12}$$

where P is the number of antennas, k is the wavenumber, a is the radius of the circle, I_p is the complex excitation coefficient of the pth element, and ϕ_p is the angle between the pth element and the x axis. At this stage, we assume that the dots in Figure 3 represent the center of the active regions located on the LP antennas. Since the active region appears on the elements that are about a quarter-wavelength long, the circle in Figure 3 has a radius that is inversely proportional to k. Consequently, f_{AF} becomes independent of frequency with the elimination of the k factor in the exponential term of (12). Finally, if f_e is almost frequency-independent, we conclude that the radiation intensity of the array f_a should also be independent of frequency to the same degree.
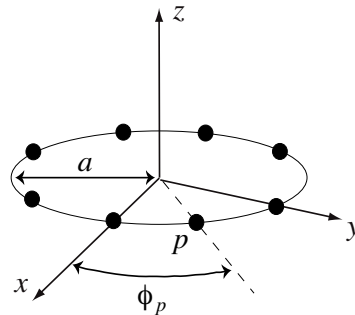

Figure 3. Configuration for a circular array, where the elements of the array are represented by the dots on a circle.

Despite the simple discussion above, the simulations show that we cannot ignore the mutual couplings between LP antennas that are located close together, as in Figure 2. To prove this, we compare radiations from the single antenna in Figure 1 with the array in Figure 2, where only the antenna on the x axis is active. Considering (11) and (12) in this case, I_p is zero for the unexcited elements, and the radiation of the array should be the same as the radiation of the single antenna. On the other hand, in Figure 4, we plotted the directive gain in the $-x$ direction with respect to frequency, and it is completely different for the array and the single antenna. Due to mutual couplings, the unexcited antennas in the array significantly modify the total radiation. The directive gain of the array oscillates much more than the single element, demonstrating a drop in the quality of frequency independence.
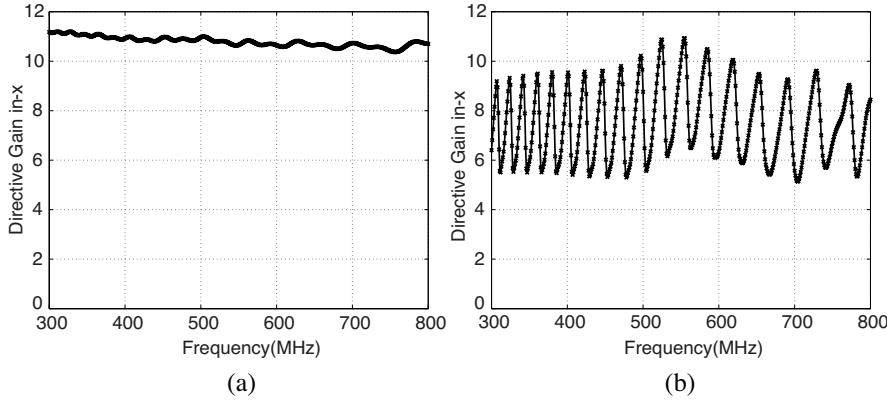

(a)   (b)

Figure 4. Directive gain in the $-x$ direction sampled with $1\,\mathrm{MHz}$ resolution for (a) the trapezoidal-tooth LP antenna in Figure 1 and (b) the circular array in Figure 2 with only the antenna on the x axis active.

We have confirmed that the oscillations in Figure 4(b) are directly related to the geometric growth factor (τ) of the LP array. Let f_i and f_{i+1} be two consecutive frequencies, at which the directive gain makes a peak. Then,

$$\frac{f_i}{f_{i+1}} \approx \tau, \tag{13}$$

which is equal to 0.95 in our case. Figyres 5(a) and (b) show the directive gain when τ becomes 0.98 and 0.85, respectively. It is clearly observed that the oscillation rate depends on τ. In fact, this relation
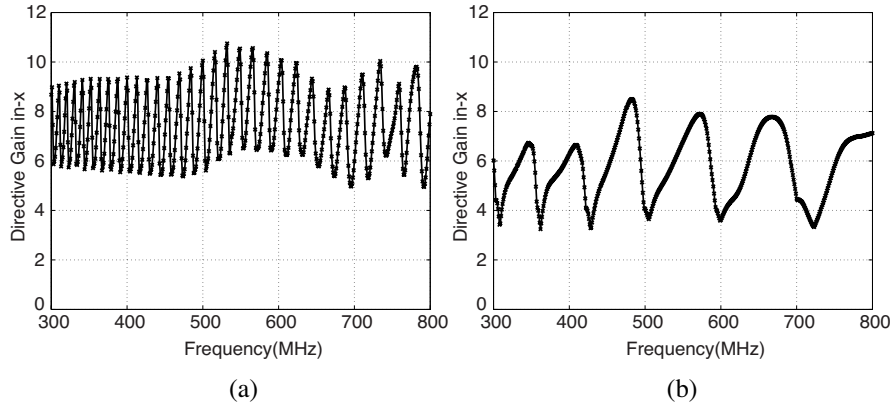
(a)   (b)

Figure 5. Directive gain in the $-x$ direction sampled with $1\,\text{MHz}$ resolution for the configuration in Figure 2 with only the antenna on the x axis active for (a) $\tau = 0.98$ and (b) $\tau = 0.85$.

also exists in the case of the single antenna in Figure 4(a). However, the active region on the single antenna moves so smoothly that the radiation characteristics change little in the intervals $[f_i, f_{i+1}]$ and the oscillation is less visible. When we examine the array configurations, we note that the mutual couplings between the antennas disturb the localization of the active region, and we see a large effect on the radiation characteristics.

4. GENETIC OPTIMIZATION OF DIRECTIVE GAIN

For the array in Figure 2, we wish to optimize the directive gain in a certain direction by selecting the best complex excitation coefficients for the antennas. In this section, we consider the optimization of the directive gain in the $-x$ direction, while the same process will be employed in Section 5 to steer the main beam. At a fixed frequency, we express the complex excitation coefficient of the pth antenna as

$$I_p = A_p \exp(i\varphi_p), \qquad p = 1, 2, 3, \tag{14}$$

where A_p and φ_p represent the amplitude and phase of the excitation, respectively. Without loss of generality, we take $\varphi_1 = 0$ and optimization is performed on five parameters. For each p, A_p can take values from 0 to 1, and for $p = 2$ and 3, φ_p can take values from $0°$ to $360°$.

Applying a discretization approach to the variables, samples are selected regularly in the intervals $[0, 1]$ and $[0, 360°]$ for A_p and φ_p,

respectively. If optimization is performed by a brute-force approach, i.e., by simply scanning the optimization space and checking every possible combination of the variables, processing time will be extremely long. For example, we discretize each variable with 10 samples. The amplitudes A_p are sampled as $0.0, 0.1, 0.2, \ldots, 0.9$, and the phases φ_p are sampled as $0°, 36°, 72°, \ldots, 324°$. The number of trials required to determine the optimum combination of the parameters is $10^5 = 100,000$ since there are five parameters, i.e., A_1, A_2, A_3, φ_2, and φ_3. If there is more than one frequency (500 in this paper), the number of trials can be extremely large. Although not every trial requires a solution with MLFMA, the brute-force approach is still not feasible; and it is even more difficult to employ the brute-force approach for more populous arrays.

We were able to perform the optimization more efficiently by using genetic algorithms. Since they have been successfully employed for many applications in electromagnetics [42–46], we will not go into the details of genetic algorithms here. Instead, we will briefly explain how we performed the optimization of the excitations:

(i) Genetic algorithms work on a *pool* of *citizens*. Each *citizen* is actually a trial, i.e., a choice for the set of variables. For example, a *citizen* in our problem may imply that $\{A_1, A_2, A_3, \varphi_2, \varphi_3\} = \{0.2, 0.4, 0.3, 36°, 108°\}$. The excitations represented by this *citizen* would be

$$I_1 = 0.2, \quad I_2 = 0.4 \exp(i36°), \quad I_3 = 0.3 \exp(i108°). \qquad (15)$$

In the beginning, the *pool* is formed by randomly created *citizens*. It then evolves as new *generations* are created. The number of *citizens* is fixed for an optimization; we use *pools* with 20–30 *citizens*.

(ii) Each *citizen* has a measure of *success*. In our case, this is the directive gain of the array in the optimization direction. *Citizens* with high *success* contribute to the construction of the new *generations*. *Citizens* with low *success* are eliminated automatically.

(iii) Each *citizen* has a *chromosome* to be used in the *breeding* process. The *chromosome* is a key to represent the values of the variables implied by the *citizen*. To evaluate the *chromosomes*, we employ one-to-one mapping to convert the given values to binary words.

(iv) The next *generation* of the *pool* is formed by the *breeding* process. For a *breeding* operation, two *citizens* with high *success* are selected randomly. These are called *parents*. Then, the binary numbers in the *chromosomes* of the *parents* are exchanged

randomly. There are various *crossover* schemes to perform the exchanges [42]. Heuristically, the two new *citizens* created by the *breeding* process and called *children* have a high probability of being more successful than their *parents*. The next *generation* is complete when all the *breeding* operations have created the required number of *children*.

(v) The *citizens* are randomly subject to *mutation*. We use a *mutation* rate of about 5 percent for each binary number in the *chromosomes*. The choice of the *mutation* rate is important since lower rates lead to slower convergence, while larger rates may prohibit the convergence all together.

(vi) As new *generations* are formed, the quality of the *pool* is expected to increase. In the extreme case, all the *citizens* in the *pool* become the same and they all possess the optimized values for the variables. Then, the *pool* is converged. However, it is usually enough to breed *generations* up to a fixed limit and take out the best *citizen* in the final *pool*. In our optimizations, we breed 50 *generations*.

By employing genetic algorithms, we can reduce the number of trials for a fixed frequency from 100,000 to about 1000–1500. This leads to a significant reduction in processing time. With numerous experiments, we have confirmed that genetic algorithms converge to optimized values that are very close to those found by the brute-force approach.

For each trial, either by brute force or genetic algorithms, a set of excitations have to be applied on the antennas to compute the directive gain. We do not perform this by solving the radiation problem for each set of excitations. Instead, we employ the superposition technique to compute the radiated fields in a more efficient way. Consider the three-element array depicted in Figure 2. For a fixed frequency, we perform a single solution with MLFMA. In this solution, only one antenna is excited with a unity excitation. Then, the complex radiated field is stored in memory to be used during the optimization. When a set of excitations is to be tested, the radiated field and its two rotated versions, i.e., rotated by $120°$ and $240°$, are multiplied with the corresponding excitation coefficients and combined into a single field. Following this superposition, directive gain is calculated from the total field. Consequently, for a circular-symmetric array, only a single solution with MLFMA is required at each frequency.

Figure 6 presents the result of the optimization by genetic algorithms for the array in Figure 2. The directive gain in the $-x$ direction is plotted with respect to frequency for two cases; when only the antenna on the x-axis is excited, and when all the antennas are
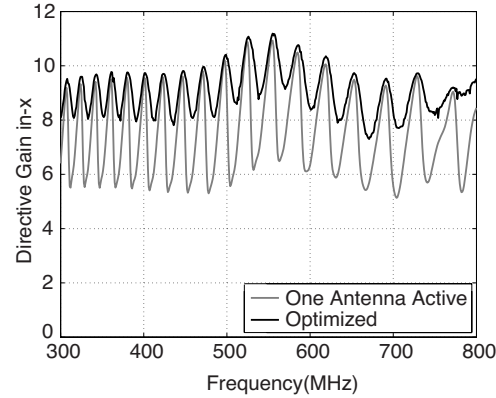
Figure 6. Directive gain in the $-x$ direction sampled with $1\,\mathrm{MHz}$ resolution for the array in Figure 2 when (a) only the antenna on the x axis is active, and (b) three antennas are active with the optimized excitations.

active with the optimized excitations. For any frequency, optimization is expected to provide increased directive gain. This is in fact the case; however optimization is even more effective at those frequencies, where the directive gain is low. Therefore, the optimization by genetic algorithms reduces the variation in the directive gain with respect to frequency, and the array becomes more frequency-independent.

5. BEAM-STEERING

Since the array in Figure 2 is rotationally symmetric, i.e., its elements are regularly spaced, it already has some beam-steering ability. Considering the optimization of the directive gain in the $-x$ ($\phi = 180°$) direction, the same directive gain can also be obtained at $\phi = 60°$ and $\phi = 300°$ by simply exchanging the excitations among the antennas. However, it is also desirable to steer the main beam in any direction within a sector between two antennas. This goal can again be achieved via optimization with genetic algorithms.

Figures 7 and 8 show the results of the optimization. Since it is easier to rotate the antenna than to change the optimization direction, we use the configurations shown at the bottom of Figure 8; the optimization angle is fixed at $\phi = 180°$ for all configurations. The array is rotated $10°$, $20°$, and $30°$ in the ϕ direction to test the beam-steering ability in a sector of $2 \times 30° = 60°$. We confirmed that a rotation in the negative direction is not required; due to symmetry, the results
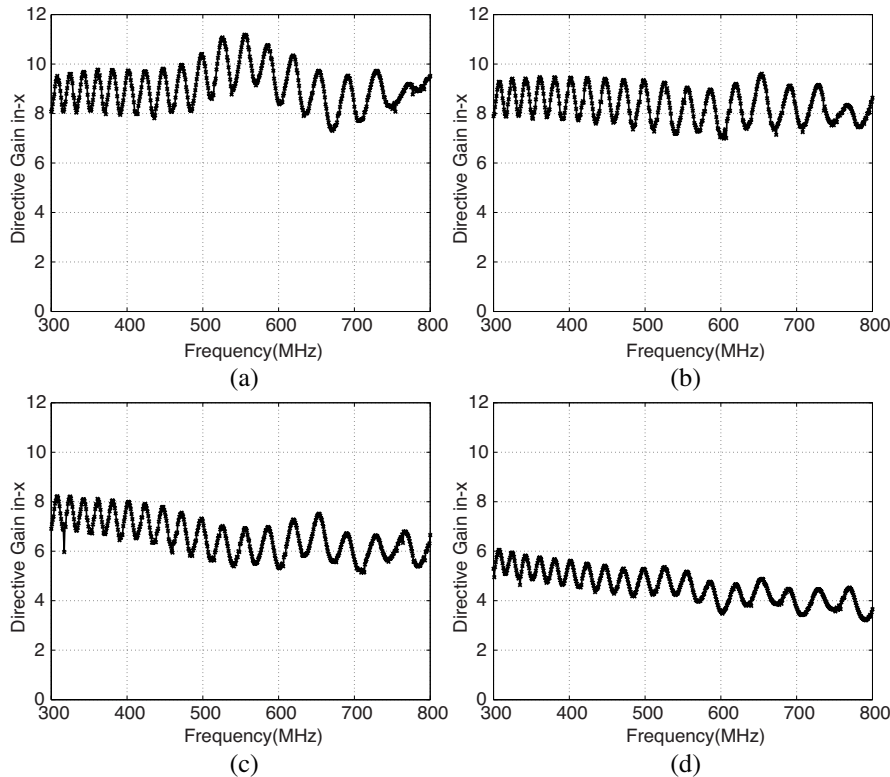
Figure 7. Optimized directive gain in the $-x$ direction sampled with 1 MHz resolution when the array in Figure 2 is rotated in the ϕ direction for (a) 0°, (b) 10°, (c) 20°, and (d) 30°.

of an optimization in the $-\phi_0$ direction can be approximated from the optimization in the $+\phi_0$ direction. In Figure 7, we observe that the optimized directive gain in the $-x$ direction drops as the antenna is rotated; this is because the main beam is not totally controllable, and it is difficult to maintain the directive gain at high levels. This is also evident in Figure 8, where the normalized far-zone radiation pattern of the array is plotted on a decibel (dB) scale for some selected frequencies and for different alignments of the array (shown at the bottom). The maximum radiation cannot be kept in the $-x$ direction when the antenna is rotated 30°. Nevertheless, the directive gain is larger than 5 up to 20°. This means that the array in Figure 2 can provide a directive gain larger than 5 in three distinct sectors, each of which has an extent of 40°. We note that this is valid for a wide frequency range from 300 MHz to 800 MHz.
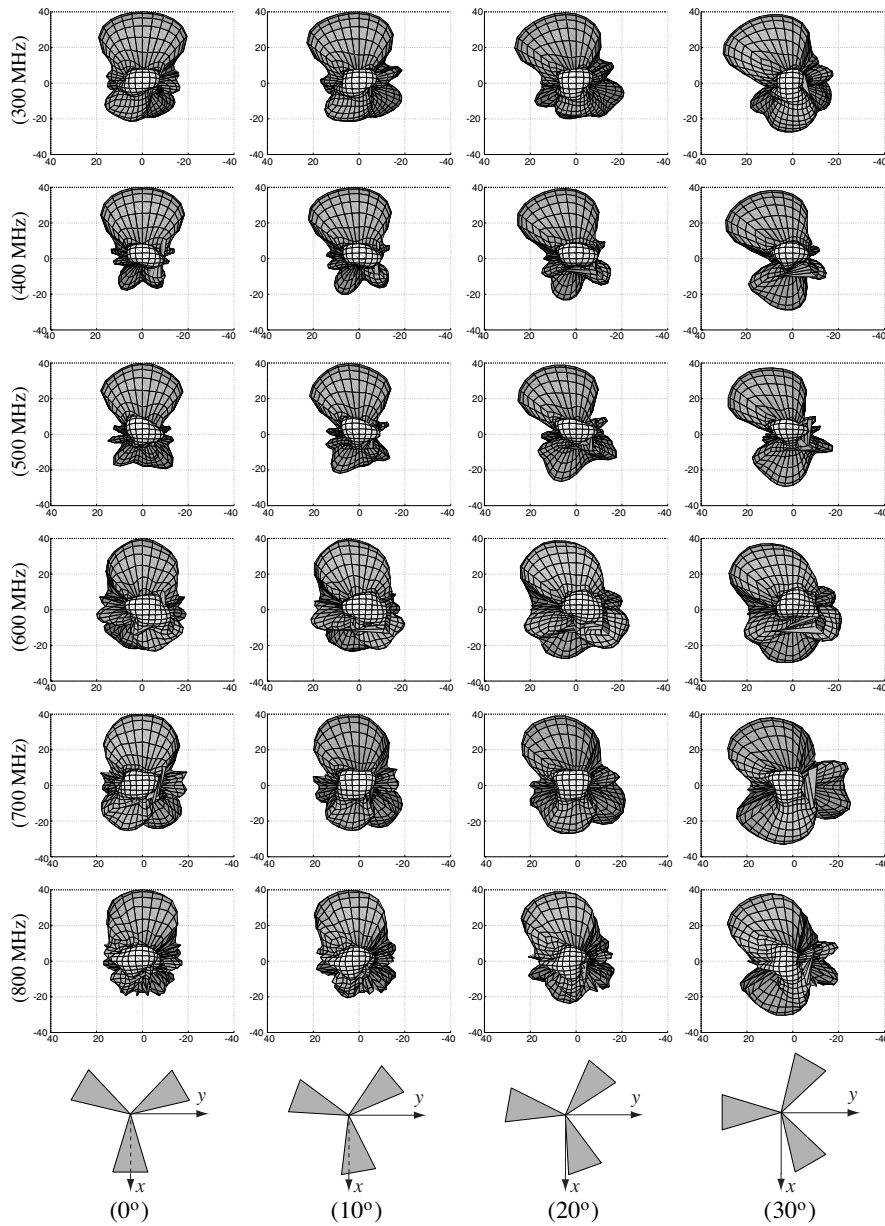
Figure 8. Normalized far-zone radiation pattern of the array in Figure 2 for various frequencies and alignments. Directive gain is optimized in the $-x$ direction.

6. CONCLUSION

In this paper, we analyze the circular arrays that are constructed by regularly spaced LP antennas in a simulation environment. These arrays show broadband characteristics and the main beam is steerable by exciting the antennas appropriately. Optimization of excitations by genetic algorithms improves the design and extends the steering ability. It is also possible to achieve broadband beam steering over wider sectors with other configurations that are not circularly symmetric; these are reported elsewhere [33].

ACKNOWLEDGMENT

REFERENCES

1. DuHamel, R. H. and D. E. Isbell, "Broadband logarithmically periodic antenna structures," *IRE National Convention Record*, Pt. 1, 119–128, May 1957.

2. Isbell, D. E., "Nonplanar logarithmically periodic antenna structures," Tech. Rep. 30, Antenna Lab., University Illinois, Urbana, Illinois, U. S. A., Feb. 1958.

3. DuHamel, R. H. and F. R. Ore, "Logarithmically periodic antenna designs," *IRE National Convention Record*, Pt. 1, 139–152, 1958.

4. Isbell, D. E., "Log-periodic dipole arrays," *IRE Trans. Antennas Propagat.*, Vol. 8, 260–267, May 1960.

5. Carrel, R. L., "Analysis and design of the log-periodic dipole antenna," Tech. Rep. 52, Antenna Lab., University Illinois, Urbana, Illinois, U. S. A., Sept. 1961.

6. Joardar, S. and A. B. Bhattacharya, "Two new ultra wideband dual polarized antenna-feeds using planar log periodic antenna and innovative frequency independent reflectors," *J. of Electromagn. Waves and Appl.*, Vol. 20, No. 11, 1465–1479, 2006.

7. Gheethan, A. A. and D. E. Anagnostou, "The design and optimization of planar LPDAs," *PIERS Online*, Vol. 4, No. 8, 811–814, 2008.

8. Jones, K. E. and P. E. Mayes, "Continuously scaled transmission lines with applications to log-periodic antennas," *IEEE Trans. Antennas Propagat.*, Vol. 17, No. 1, 2–9, Jan. 1969.

9. Kyle, R. H., "Mutual coupling between log-periodic antennas," *IEEE Trans. Antennas Propagat.*, Vol. 18, No. 1, 15–22, Jan. 1970.

10. Wolter, J., "Solution of Maxwell's equations for log-periodic dipole antennas," *IEEE Trans. Antennas Propagat.*, Vol. 18, No. 6, 734–740, Nov. 1970.

11. Oakes, C. R. and K. G. Balmain, "Optimization of the loop-coupled log-periodic antenna," *IEEE Trans. Antennas Propagat.*, Vol. 21, No. 2, 148–153, Mar. 1973.

12. De Vito, G. and G. B. Stracca, "Comments on the design of log-periodic dipole antennas," *IEEE Trans. Antennas Propagat.*, Vol. 21, No. 3, 303–308, May 1973.

13. De Vito, G. and G. B. Stracca, "Further comments on the design of log-periodic dipole antennas," *IEEE Trans. Antennas Propagat.*, Vol. 22, 714–718, Sept. 1974.

14. Butson, P. C. and G. T. Thompson, "A note on the calculation of the gain of log-periodic dipole antennas," *IEEE Trans. Antennas Propagat.*, Vol. 24, 105–106, Jan. 1976.

15. Paul, A. and I. Gupta, "An analysis of log-periodic antenna with printed dipoles," *IEEE Trans. Microwave Theory Tech.*, Vol. 29, No. 2, 114–117, Feb. 1981.

16. Tranquilla, J. M. and K. G. Balmain, "Analysis of the loop-coupled log-periodic dipole array," *IEEE Trans. Antennas Propagat.*, Vol. 31, No. 2, 253–260, Mar. 1983.

17. Gong, Z. and K. G. Balmain, "Reduction of the anomalous resonances of symmetric log-periodic dipole antennas," *IEEE Trans. Antennas Propagat.*, Vol. 34, No. 12, 1404–1410, Dec. 1986.

18. Peixeiro, C., "Design of log-periodic dipole antennas," *Proc. IEE*, Vol. 135, Pt. H, No. 2, 98–102, Apr. 1988.

19. Hilbert, R., M. A. Tilston, and K. G. Balmain, "Resonance phenomena of log-periodic antennas: Characteristic-mode analysis," *IEEE Trans. Antennas Propagat.*, Vol. 37, No. 10, 1224–1234, Oct. 1989.

20. Baker, D. C. and T. G. Reuss, "An investigation of the design of a log-periodic dipole array with low side-lobe levels for broadcast applications," *IEEE Trans. Broadcasting*, Vol. 36, No. 1, 89–93, Mar. 1990.

21. Hassan, M. A., A. Al-Jabri, and K. Al-Hakbani, "Point-matching method for reduction of anomalous radiation of log-periodic dipole

array," *Electron. Lett.*, Vol. 27, No. 15, 1315–1317, July 1991.

22. Wakabayashi, R., K. Shimada, H. Kawakami, and G. Sato, "Circularly polarized log-periodic dipole antenna for EMI measurements," *IEEE Trans. Electromagn. Compat.*, Vol. 41, No. 2, 93–99, May 1999.

23. Excell, P. S., A. D. Tinniswood, and R. W. Clarke, "An independently fed log-periodic antenna for directed pulsed radiation," *IEEE Trans. Electromagn. Compat.*, Vol. 41, No. 4, 344–349, Nov. 1999.

24. Bell, R. L., C. T. Elfving, and R. E. Franks, "Near-field measurements on a logarithmically periodic antenna," *IRE Trans. Antennas Propagat.*, Vol. 8, 559–565, Nov. 1960.

25. Liang, C. S. and Y. T. Lo, "A multipole-field study for the multiarm log-spiral antennas," *IEEE Trans. Antennas Propagat.*, Vol. 16, No. 6, 656–664, Nov. 1968.

26. Lee, S. H. and K. K. Mei, "Analysis of zigzag antennas," *IEEE Trans. Antennas Propagat.*, Vol. 18, No. 6, 760–764, Nov. 1970.

27. Hall, P. S., "Multioctave bandwidth log-periodic microstrip antenna array," *Proc. IEE*, Vol. 133, Pt. H, No. 2, 127–136, Apr. 1986.

28. Smith, H. K. and P. E. Mayes, "Log-periodic array of dual-feed microstrip patch antennas," *IEEE Trans. Antennas Propagat.*, Vol. 39, No. 12, 1659–1664, Dec. 1991.

29. Tammen, D. J., J. M. Bowen, and P. E. Mayes, "Numerical studies of the sinuous spiral antenna," *1993 IEEE Int. Antennas Propagat. Symp. Dig.*, Vol. 31, 446–449, June 1993.

30. Wu, S.-C. and N. G. Alexopoulos, "Broadband microstrip antennas on electrically thick substrates *J. of Electromagn. Waves and Appl.*, Vol. 7, No. 1, 123–146, 1993.

31. Ergül, Ö. and L. Gürel, "Log-periodic antenna design using electromagnetic simulations," *Proc. IEEE Antennas and Propagation Soc. Int. Symp.*, Vol. 1, 245–248, 2003.

32. Ergül, Ö. and L. Gürel, "Nonplanar trapezoidal-tooth log-periodic antennas: design and electromagnetic modelling," *Radio Science*, Vol. 40, RS5010, doi:10.1029/2004RS003215, Oct. 2005.

33. Ergül, Ö. and L. Gürel, "Modeling and synthesis of circular-sectoral arrays of log-periodic antennas using multilevel fast multipole algorithm and genetic algorithms," *Radio Science*, Vol. 42, RS3018, doi:10.1029/2006RS003567, June 2007.

34. Glisson, A. W. and D. R. Wilton, "Simple and efficient numerical methods for problems of electromagnetic radiation and scattering

from surfaces," *IEEE Trans. Antennas Propagat.*, Vol. 28, No. 5, 593–603, Oct. 1980.

35. Harrington, R. F., *Field Computation by Moment Methods*, IEEE Press, 1993.

36. Rao, S. M., D. R. Wilton, and A. W. Glisson, "Electromagnetic scattering by surfaces of arbitrary shape," *IEEE Trans. Antennas Propagat.*, Vol. 30, 409–418, May 1982.

37. Song, J., C.-C. Lu, and W. C. Chew, "Multilevel fast multipole algorithm for electromagnetic scattering by large complex objects," *IEEE Trans. Antennas Propagat.*, Vol. 45, No. 10, 1488–1493, Oct. 1997.

38. Chew, W. C., J.-M. Jin, E. Michielssen, and J. Song, *Fast and Efficient Algorithms in Computational Electromagnetics*, Artech House, Boston, MA, 2001.

39. Stutzman, W. L. and G. A. Thiele, *Antenna Theory and Design*, Chapter 6, Wiley, New York, 1981.

40. Kraus, J. D., *Antennas*, Chapter 15, McGraw-Hill, Singapore, 1988.

41. Balanis, C. A., *Antenna Theory*, Chapter 11, Wiley, New York, 1997.

42. Rahmat-Samii, Y. and E. Michielssen, *Electromagnetic Optimization by Genetic Algorithms*, Wiley, New York, 1999.

43. Fisher, S. E., D. S. Weile, and E. Michielssen, "Pareto genetic algorithm based optimization of log-periodic monopole arrays mounted on realistic platforms," *J. of Electromagn. Waves and Appl.*, Vol. 13, 571–598, 1999.

44. Pissoort, D., H. Rogier, F. Olyslager, and D. De Zutter, "Optimization of a microstrip antenna with a genetic algorithm for use as a ground penetrating radar," *J. of Electromagn. Waves and Appl.*, Vol. 17, No. 8, 1197–1216, 2003.

45. Sijher, T. S. and A. A. Kishk, "Antenna modeling by infinitesimal dipoles using genetic algorithms *Progress In Electromagnetics Research*, PIER 52, 225–254, 2005.

46. Chung, Y. C. and R. Haupt, "Log-periodic dipole array optimization," *J. of Electromagn. Waves and Appl.*, Vol. 15, No. 9, 1269–1280, 2001.